Mesoporous Nanoparticles | Hot Paper

DOI: 10.1002/ange.201307126

All-Metal Mesoporous Nanocolloids: Solution-Phase Synthesis of Core–Shell Pd@Pt Nanoparticles with a Designed Concave Surface

*Hamed Ataee-Esfahani, Masataka Imura, and Yusuke Yamauchi**

In recent years, much effort has been made towards the synthesis of shape- and size-controlled metal colloidal nanoparticles that possess novel physical and chemical properties.[1] Previous synthetic methods have employed preformed metal seeds and/or various chemical additives. In almost all of these cases, complicated procedures, including several steps and/or high pressure and temperature conditions, are required.[2] Bimetallic nanoparticles have often shown superior catalytic activity over their monometallic counterparts, owing to the synergetic effect of the second metal.[3] However, heterogeneous bimetallic nanoparticles, such as core–shell structures, are more difficult to prepare than monometallic nanoparticles. This is due to the complicated synthetic conditions caused by the difference in the reduction rate of metal salts and the different tendencies of structural directing agents for interaction with metal surfaces. To date, few methods have been developed for the formation of shallow concavities on metal nanoparticles under controlled conditions,[4] but the facile synthesis of metal nanoparticles with mesopores, which provide a high surface-to-volume ratio, is still a challenging issue. Our target in this study is the synthesis of mesoporous metal nanoparticles with high indexed facets, which can provide many catalytically active sites for catalytic reactions, especially in electrooxidation reactions.

Much attention has recently been paid to the synthesis of mesoporous silica nanoparticles because of their different industrial and technological applications. The properties of these mesoporous nanoparticles can be greatly affected by particle sizes. Reducing the particle sizes to the nanometer range (less than 100 nm) enables sustained colloidal suspensions with interesting properties to be made. Mesoporous nanoparticles are highly useful in important applications, such as adsorption, catalysis, drug delivery and energy storage.[5] However, the compositions of mesoporous nanoparticles previously reported have been limited to metal oxides (such as silica or titania)[6] and carbon,[7] which seriously devalues the possible application range of mesoporous nanoparticles. Mesoporous nanoparticles with different compositions can realize a variety of functions. In particular, all-metal mesoporous nanoparticles are highly useful for a wide range of electrochemical applications. There are two main methods for the preparation of all-metal mesoporous materials: the lyotropic liquid crystalline approach[8] and the hard-templating approach (replication method).[9] However, these approaches are not applicable as general strategies for the synthesis of monodispersed mesoporous metal nanoparticles.

The main problem in the synthesis of mesoporous metals is the difficulty of spontaneously forming a concave morphology, which is generally not favored by thermodynamics. In a general solution-phase synthesis, metal nanoparticles tend to show a faceted crystal morphology observed with low-index surfaces, such as {111} and {100} planes.[10] The essence of our proposed method in this study is to take the advantage of the self-assembly of surfactants into spherical micelles and employ them as templates for the synthesis of mesoporous metal nanoparticles. Herein, we demonstrate the synthesis of bimetallic mesoporous Pd@Pt nanoparticles. The mesoporous structures in the Pd@Pt nanoparticles provide a high surface area and many catalytically active sites on a concave surface. Compared to irregular morphology, nanoparticle morphology can contribute to facilitate the transportation of reactants/products to greatly enhance the electrocatalytic activity of the mesoporous Pd@Pt nanoparticles.

To prepare mesoporous metal nanoparticles, Pluronic F127 was ultrasonically dissolved in the precursor solution containing Pt and Pd sources and hydrochloric acid. After adding ascorbic acid (AA) as a reducing agent, the mixture was continuously sonicated. As the reaction proceeded, the solution color changed to black, as shown in Figure S1 in the Supporting Information. The obtained nanoparticles were well dispersed in water without any precipitation, indicating a high-quality colloidal solution. The final product was collected and washed with acetone and water in consecutive washing/centrifugation cycles for the removal of undeposited metal sources and surfactant. The detailed experimental procedure is given in the Supporting Information.

Figure 1 shows scanning electron microscopy (SEM) and transmission electron microscopy (TEM) images of the obtained nanoparticles synthesized under standard conditions. The size distribution of the nanocolloids was 45 ± 5.0 nm, with an average size of 45 nm. As shown in Figure 1c,d, uniform mesopores were confirmed on the nanoparticle surface. It should be noted that the mesopores on the outer surface were hemispherical and showed well-defined concavities. Low-angle X-ray diffraction (XRD) profiles for mesoporous Pd@Pt nanoparticles showed one broad peak, meaning that the uniformly sized pores are closely packed

[*] Dr. H. Ataee-Esfahani, Dr. M. Imura, Prof. Dr. Y. Yamauchi
World Premier International (WPI) Research Center for Materials Nanoarchitectonics (MANA), National Institute for Materials Science (NIMS), 1-1 Namiki, Tsukuba, Ibaraki 305-0044 (Japan)
E-mail: Yamauchi.Yusuke@nims.go.jp
Homepage: http://www.yamauchi-labo.com
Prof. Dr. Y. Yamauchi
Faculty of Science and Engineering, Waseda University
3-4-1 Okubo, Shinjuku, Tokyo 169-8555 (Japan)

Supporting information for this article is available on the WWW under http://dx.doi.org/10.1002/anie.201307126.

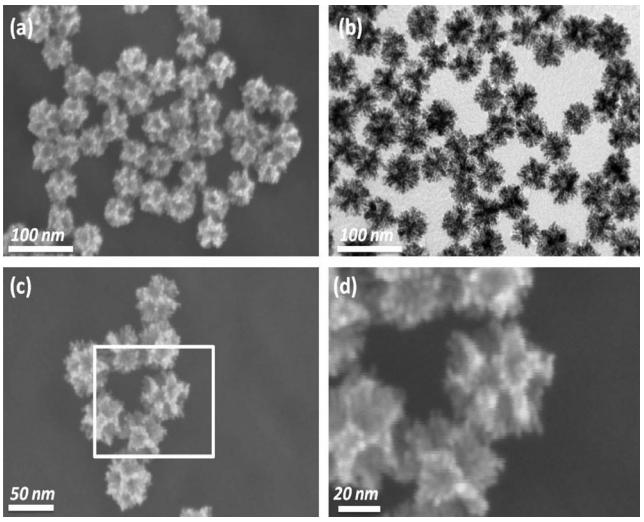

Figure 1. a, c, and d) SEM and b) TEM images of mesoporous Pd@Pt nanoparticles. d) Enlarged image of the square area marked in (c).

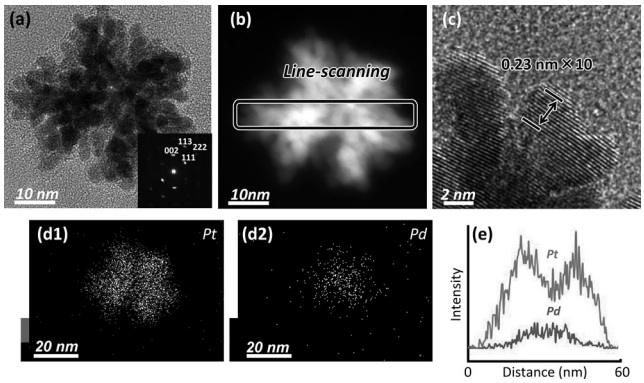

Figure 3. a) Bright-field and b) dark-field TEM images for mesoporous Pd@Pt nanoparticles prepared under the standard conditions. c) High magnification TEM image of the edge part of mesoporous Pd@Pt nanoparticles. Inset image in (a) shows the selected-area electron diffraction patterns obtained from one particle. d) Pt (d1) and Pd (d2) elemental mapping of mesoporous Pd@Pt nanoparticles. e) Elemental distribution of Pt and Pd in the highlighted regions of (b).

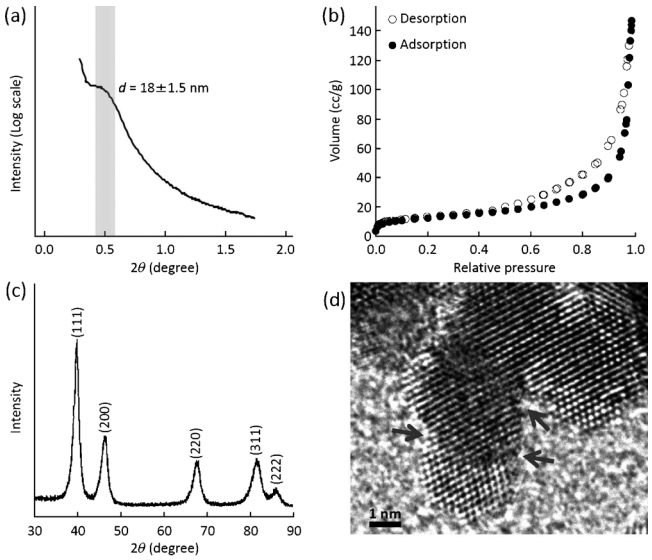

Figure 2. a) Low-angle XRD profile, b) N_2 adsorption-desorption isotherm, c) high-angle XRD profile, and d) highly magnified TEM image of mesoporous Pd@Pt nanoparticles. The "neck" portion of the connected particles has concave shapes (indicated by arrows).

(Figure 2a). An N_2 adsorption–desorption isotherm gave a large surface area of 40 $m^2 g^{-1}$ (Figure 2b).

For further study of the nanoparticles, high resolution TEM was used to characterize an individual particle (Figure 3a). The pores and their walls were clearly distinguished because of differences in the contrast. The walls were made by assembly of fine nanoparticles (with 2–3 nm) and the well-developed branched structure is observed in Figure 3a,b. Thus, it clearly shows dual porosity in the nanoparticles: small pores (coming from highly branched structure in the walls) and large mesopores. Selected-area electron diffraction (ED) patterns of an individual nanoparticle (inset of Figure 3a) showed almost single-crystal-like reflections indexed to the ⟨1-10⟩ zone axis of Pt face-centered cubic (*fcc*) crystal. The observed lattice fringes were coherently extended over the entire nanoparticle. These observed fringes with spacing of 0.23 nm were in agreement with a (111) plane spacing of Pt *fcc* crystal (Figure 3c). Because of the extremely high lattice match of Pt and Pd (99.23%),[11] no obvious grain boundaries between Pt and Pd were observed. As shown in Figure 2c, the wide-angle XRD profile was also assigned to (111), (200), (220), (311), and (222) diffractions of a *fcc* crystal structure as a single phase. All of these results show that, even though the core and shell are compositionally different, the crystallographic structure is uniform and coherent over the entire nanoparticle. As seen in the highly magnified TEM image (Figure 2d), each nanoparticle showed a bumpy surface full of valency unsaturated atoms in edge and kinks, which provide many catalytically active sites. Furthermore, the connection of the nanoparticles with a coherent crystal lattice results in a concave surface topology with a large number of steps.

The elemental mapping (Figure 3d) and line-scanning data (Figure 3e) clearly revealed that Pd was concentrated in the particle center, whereas Pt was concentrated at the outer edge of the nanoparticle. This elemental distribution of Pd and Pt confirmed the formation of a Pd@Pt core-shell structure (core rich in Pd and shell rich in Pt). The core size was around 27 nm. The Pd content in the nanoparticles was measured to be 15 atomic%, which coincided with that measured by inductively coupled plasma (ICP) analysis. Low-magnification TEM and SEM images (Figure S2) clearly show that nanocolloids are remarkably uniform in size and shape without any formation of by-products, demonstrating the high-yield (100%) synthesis of the Pd@Pt nanoparticles.

To elucidate the formation mechanism of the Pd@Pt nanoparticles, reaction progress was studied stage by stage using TEM images (Figure S3). The obtained images provide insight into the formation mechanism of the nanoparticles. In the present system, in spite of the fact that the standard reduction potential for Pt ions ($[PtCl_4]^{2-}$/Pt: +0.755 V vs. SHE) is more positive than that for Pd ions ($[PdCl_4]^{2-}$/Pd:

+0.591 V vs. SHE), Pd complexes have a higher reduction rate than Pt ones. Therefore, the reduction of Pd complexes preferentially occurs in a short time to form Pd-rich initial metal seeds (Figure S3a). Similar anomalous behavior has been previously reported for the codeposition of Pd and Pt[12a,b] and other bimetallic/trimetallic systems.[12c–e] Owing to the interaction between the hydrophobic PPO groups and the metal surface,[13] the F127 molecules adsorbed on the primary metal seeds serve as a stabilizer for monodispersed nanoparticles. Because the present surfactant concentration is over critical micelle concentration (CMC), the surfactants dissolved in the solution form the spherical micelles. The metal aqua complexes dissolving in the solution are incorporated in the PEO shell region of the micelles.[14] During further deposition and subsequent overgrowth of Pt on Pd seeds, the F127 micelles with metal–aqua complexes approach the seeds and directly act as a structural directing agent to form well-defined concave morphology with an open pore structure.

As clearly seen in time-dependent TEM observation (Figure S3), each particle gradually grew. After a period of 3 h, the Pt shell growth was terminated and the size and morphology of nanoparticles no longer changed. As mentioned above, electron diffraction (ED) taken from one particle showed very intense spots completely assignable to a single *fcc* crystal (Figure 3a), which is also important evidence of continuous epitaxial growth from the seed.

The effect of surfactant concentration on the final product was also investigated (Figure S4). When the surfactant concentration in the precursor solution was decreased (up to 0.03 wt%), a mixture of porous and nonporous particles were observed (Figure S4a,b). Most of the particles were agglomerated because the amount of surfactants (as stabilizer) was not enough to inhibit particle aggregation. When the precursor solution was prepared either by adding extremely diluted surfactant concentration (below CMC) or without adding any surfactant, the mesoporous structure on the surface completely disappeared (Figure S4c,d). Hence, our observation shows that the concentration of F127 is a critical parameter for the formation of well-dispersed mesoporous nanoparticles. In this approach, the size of the Pd-rich core was easily tuned by changing the molar ratio of Pt/Pd in the precursor solution. Figure S5 shows TEM images of Pd@Pt nanoparticles in which the molar ratio of Pt/Pd changed from 9.0 (typical condition) to 4.0. As shown by elemental analysis, the size of the Pd-rich core was around 47 nm which was around 1.7 times larger than that of the typical sample.

In the present reaction system, ascorbic acid is used as a reducing agent, and is oxidized according to the following equilibrium equation: $C_6H_8O_6 \leftrightarrow C_6H_6O_6 + 2H^+ + 2e^-$. Hence, the reducing capacity of ascorbic acid can be adjusted by precise control of pH (acidity) of the precursor solution. The synthesis progress was monitored by UV/Vis absorption spectroscopy at different reaction times (Figure S6a). The relative concentration of precursor solution was evaluated from the characteristic absorption peak of Pt complexes centered at 390 nm. At high pH, relative concentration immediately decreased in 5 min, indicating the rapid reduction of metal ions. With further increasing the reaction time, the Pt concentration gradually decreased. All Pt ions were completely consumed after 1 hour of reaction. In contrast, the reduction rate at low pH was very slow. The relative concentration gradually declined in 4 h. Thus, the reaction time at low pH (4 h) was much longer than that at high pH (1 hour). The reduction rate in both cases was also visibly monitored through the color evolution of the reaction solution (Figure S6b). At high pH, the color of the reaction solution immediately changed from an initial yellow color to black in 5 min, thus indicating the formation of nanoparticles, while at low pH the solution color gradually turned black in 60 min. From the above results, it was revealed that the reduction rate of metal ions dramatically decreased when adding acid to the precursor solution.

Figure S7a shows SEM images of the obtained product prepared by a precursor solution at high pH. The product possessed a highly branched (dendritic) structure without any uniform-sized mesopores, which is in contrast to the obtained nanoparticles prepared under the low pH system (Figure S7b). At low pH, slow metal growth provides enough time for surfactant micelles to adhere to the metal seeds and effectively act as a template for the further growth of the initial seeds. This slow growth mechanism is completely different from the formation of dendritic Pt-based nanostructures at high pH under fast-growth conditions. The relatively high rate of metal ion reduction at high pH leads to instantaneous nucleation in a short time and formation of dendritic particles with a highly branched structure. This mechanism was recently developed by us for the synthesis of dendritic Pt nanostructures.[15] Hence, such pH control of the precursor solution is important for the formation of uniform-sized mesopores.

As a preliminary demonstration of the electrocatalytic activity of mesoporous Pd@Pt nanoparticles towards the oxidation of methanol, the electrocatalytic activity was investigated using cyclic voltammograms in a H_2SO_4/CH_3OH (0.5 M/0.5 M) electrolyte solution (Figure S8). To make a comparison, the electrocatalytic activity of commercially available Pt black (PtB) and dendritic Pt nanoparticles (shown in Figure S9)[16] was also examined. All the obtained currents were normalized to the mass of loaded Pt. As seen in Figure S8a, mesoporous Pd@Pt nanoparticles showed the highest current density (395 $mA\,mg^{-1}$). This value is 1.7 times higher than that of dendritic Pt nanoparticles (234 $mA\,mg^{-1}$) and also around 4.2 times higher than that of PtB (95 $mA\,mg^{-1}$). As shown in Figure S8b, the current density of mesoporous Pd@Pt nanoparticles was significantly higher than those of other state-of-the-art dendritic Pt nanoparticles previously reported, such as Pt–Ru nanoparticles[17] and Au@Pt nanoparticles.[18]

The value of I_f/I_b (defined as the ratio between forward and backward current densities) can be used as an indicator of the CO tolerance of Pt catalysts in the methanol oxidation reaction (MOR).[19] Mesoporous Pd@Pt nanoparticles exhibited superior poison tolerance and the I_f/I_b value was 1.08, which is higher than those of dendritic Pt nanoparticles (0.96) and PtB (0.85). Furthermore, a remarkably negative shift of the onset potential (ca. 100 mV) was also observed in comparison with dendritic Pt nanoparticles and PtB. As mentioned above, the atoms of Pd and Pt are highly miscible,

and the Pd atoms in the Pd-rich core coherently match with the lattice structure of the exterior Pt-rich shell, resulting in the formation of the inserted pseudo Pt–Pd alloy heterointerface, of which the Pd (as an oxophilic element) can enhance the removal of adsorbed CO on neighboring Pt atoms by adsorbing oxygen-containing species.[20] The formation of a Pt–Pd alloy might be also helpful for facilitating the C–H cleavage reaction in methanol decomposition.[21] The above two effects play a key role for acceleration of methanol oxidation reaction.

In addition, we discussed the topological interest of our mesoporous nanoparticles on the basis of activity for the methanol oxidation reaction. From the N_2 adsorption isotherm, the surface area of PtB was measured to be around $20\ m^2 g^{-1}$. When the electrocatalytic activity was normalized by the surface area, the activity of mesoporous Pd@Pt nanoparticles was still around twice that of Pt black. From this result, it can be understood that the enhanced activity observed here is attributable to the increase of active sites. Generally, defect sites and step edges enhance dissociation of water and methanol molecules.[22] As seen in Figure 2d, the mesoporous structure provides not only high surface area but also rich atomic steps with concave surface topology, which probably enhanced cleavage of C–H and O–H bonds in methanol decomposition.

In conclusion, we have demonstrated a facile solution-phase synthesis of colloidal mesoporous Pd@Pt nanoparticles with uniform-sized mesopores. The key factor in the proposed method is the assembly of surfactant micelles. By slow reduction of metal species at strong acidic media, F127 micelles can directly act as a template to form the mesopores. Because of the higher tendency of Pd species toward reduction, the reduction of Pd species preferentially occurs to form core–shell Pd@Pt nanocolloids. This new approach enables us to synthesize all-metal mesoporous nanoparticles in one-step, which cannot be achieved by either the previous methods for synthesis of metal nanoparticles (such as seeded growth and site-specific etching) or those for the synthesis of mesoporous metals (such as soft- or hard-templating methods). Mesoporous metal nanoparticles with a concave surface can provide not only a high surface area but also abundant active sites for catalytic reactions. Because of the key role of size and composition of mesoporous nanoparticles in their catalytic properties, the synthesis of mesoporous nanocolloids with different sizes and compositions and their effect on the catalytic properties will be studied in future. Our approach, based on an all-wet process in dilute surfactant solution, is widely applicable to other metal and alloy systems and also will be utilized as a promising approach for industrial mass-production.

Received: August 13, 2013
Published online: November 15, 2013

Keywords: colloids · mesoporous materials · nanoparticles · surfactants · template synthesis

[1] a) M. Chen, B. Wu, J. Yang, N. Zheng, *Adv. Mater.* **2012**, *24*, 862; b) H. Zhang, M. Jin, Y. Xia, *Angew. Chem.* **2012**, *124*, 7774; *Angew. Chem. Int. Ed.* **2012**, *51*, 7656.

[2] a) L. Zhang, D. Chen, Z. Jiang, J. Zhang, S. Xie, Q. Kuang, Z. Xie, L. Zheng, *Nano Res.* **2012**, *5*, 181; b) X. Huang, S. Tang, H. Zhang, Z. Zhou, N. Zheng, *J. Am. Chem. Soc.* **2009**, *131*, 13916; c) Z. Zhang, J. Hui, Z. Liu, X. Zhang, J. Zhuang, X. Wang, *Langmuir* **2012**, *28*, 14845; d) X. Huang, Z. Zhao, J. Fan, Y. Tan, N. Zheng, *J. Am. Chem. Soc.* **2011**, *133*, 4718; e) Y. W. Lee, M. Kim, Z. H. Kim, S. W. Han, *J. Am. Chem. Soc.* **2009**, *131*, 17036; f) S. W. Kang, Y. W. Lee, Y. Park, B. S. Choi, J. W. Hong, K. H. Park, S. W. Han, *ACS Nano* **2013**, *7*, 7945.

[3] a) H. L. Jiang, Q. Xu, *J. Mater. Chem.* **2011**, *21*, 13705; b) A. X. Yin, X. Q. Min, Y. W. Zhang, C. H. Yan, *J. Am. Chem. Soc.* **2011**, *133*, 3816; c) H. Ataee-Esfahani, J. Liu, M. Hu, N. Miyamoto, S. Tominaka, K. C. W. Wu, Y. Yamauchi, *Small* **2013**, *9*, 1047; d) S. H. Zhou, G. S. Jackson, B. Eichhorn, *Adv. Funct. Mater.* **2007**, *17*, 3099; e) J. Gu, Y. W. Zhang, F. Tao, *Chem. Soc. Rev.* **2012**, *41*, 8050.

[4] a) C. J. DeSantis, A. C. Sue, M. M. Bower, S. E. Skrabalak, *ACS Nano* **2012**, *6*, 2617; b) C. L. Lu, K. S. Prasad, H. L. Wu, J. A. A. Ho, M. H. Huang, *J. Am. Chem. Soc.* **2010**, *132*, 14546; c) H. Zhang, W. Li, M. Jin, J. Zeng, T. Yu, D. Yang, Y. Xia, Y. N. Xia, *Nano Lett.* **2011**, *11*, 898.

[5] a) T. Yang, J. Liu, Y. Zheng, M. J. Monteiro, S. Z. Qiao, *Chem. Eur. J.* **2013**, *19*, 6942; b) J. Liu, H. Q. Yang, F. Kleitz, Z. G. Chen, T. Yang, E. Strounina, G. Q. Lu, S. Z. Qiao, *Adv. Funct. Mater.* **2012**, *22*, 591; c) C. Urata, Y. Aoyama, A. Tonegawa, Y. Yamauch, K. Kuroda, *Chem. Commun.* **2009**, 5094; d) J. Kobler, T. Bein, *ACS Nano* **2008**, *2*, 2324; e) J. M. Rosenholm, C. Sahlgren, M. Lindén, *Nanoscale* **2010**, *2*, 1870.

[6] a) C. E. Fowler, D. Khushalani, B. Lebeau, S. Mann, *Adv. Mater.* **2001**, *13*, 649; b) T. W. Kim, P. W. Chung, V. S. Y. Lin, *Chem. Mater.* **2010**, *22*, 5093; c) V. Cauda, A. Schlossbauer, J. Kecht, A. Zürner, T. Bein, *J. Am. Chem. Soc.* **2009**, *131*, 11361; d) X. Huang, X. Teng, D. Chen, F. Tang, J. He, *Biomaterials* **2010**, *31*, 438; e) T. Suteewong, H. Sai, J. Lee, M. Bradbury, T. Hyeon, S. M. Gruner, U. Wiesner, *J. Mater. Chem.* **2010**, *20*, 7807; f) J. E. Lee, N. Lee, H. Kim, J. Kim, S. H. Choi, J. H. Kim, T. Kim, I. C. Song, S. P. Park, W. K. Moon, T. Hyeon, *J. Am. Chem. Soc.* **2010**, *132*, 552; g) J. Xiao, T. Peng, R. Li, Z. Peng, C. Yan, *J. Solid State Chem.* **2006**, *179*, 1161.

[7] a) Y. Fang, D. Gu, Y. Zou, Z. Wu, F. Li, R. Che, Y. Deng, B. Tu, D. Zhao, *Angew. Chem.* **2010**, *122*, 8159; *Angew. Chem. Int. Ed.* **2010**, *49*, 7987; b) T. W. Kim, P. W. Chung, I. I. Slowing, M. Tsunoda, E. S. Yeung, V. S. Y. Lin, *Nano Lett.* **2008**, *8*, 3724; c) Z. Wang, F. Li , A. Stein, *Nano Lett.* **2007**, *7*, 3223; d) M. Li, J. Xue, *J. Colloid Interface Sci.* **2012**, *377*, 169; e) J. Schuster, G. He, B. Mandlmeier, T. Yim, K. T. Lee, T. Bein, L. F. Nazar, *Angew. Chem.* **2012**, *124*, 3651; *Angew. Chem. Int. Ed.* **2012**, *51*, 3591.

[8] a) G. S. Attard, C. G. Goltner, J. M. Corker, S. Henke, R. H. Templer, *Angew. Chem.* **1997**, *109*, 1372; *Angew. Chem. Int. Ed. Engl.* **1997**, *36*, 1315; b) G. S. Attard, P. N. Bartlett, N. R. B. Coleman, J. M. Elliott, J. R. Owen, J. H. Wang, *Science* **1997**, *278*, 838; c) Y. Yamauchi, A. Takai, T. Nagaura, S. Inoue, K. Kuroda, *J. Am. Chem. Soc.* **2008**, *130*, 5426; d) Y. Yamauchi, A. Sugiyama, R. Morimoto, A. Takai, K. Kuroda, *Angew. Chem.* **2008**, *120*, 5451; *Angew. Chem. Int. Ed.* **2008**, *47*, 5371.

[9] a) H. J. Shin, R. Ryoo, Z. Liu, O. Terasaki, *J. Am. Chem. Soc.* **2001**, *123*, 1246; b) Z. Liu, O. Terasaki, T. Ohsuna, K. Hiraga, H. J. Shin, R. Ryoo, *ChemPhysChem* **2001**, *2*, 229; c) Z. Liu, Y. Sakamoto, T. Ohsuna, K. Hiraga, O. Terasaki, C. H. Ko, H. J. Shin, R. Ryoo, *Angew. Chem.* **2000**, *112*, 3237; *Angew. Chem. Int. Ed.* **2000**, *39*, 3107; d) X. J. Guo, C. M. Yang, P. H. Liu, M. H. Cheng, K. J. Chao, *J. Cryst. Growth Des.* **2005**, *5*, 33; e) K. J.

Chao, Y. P. Chang, Y. C. Chen, A. S. Lo, T. H. Phan, *J. Phys. Chem. B* **2006**, *110*, 1638.
[10] A. Chen, P. Holt-Hindle, *Chem. Rev.* **2010**, *110*, 3767.
[11] a) B. Lim, M. J. Jiang, P. H. C. Camargo, E. C. Cho, J. Tao, X. M. Lu, Y. M. Zhu, Y. N. Xia, *Science* **2009**, *324*, 1302; b) Z. M. Peng, H. Yang, *J. Am. Chem. Soc.* **2009**, *131*, 7542.
[12] a) L. Wang, Y. Nemoto, Y. Yamauchi, *J. Am. Chem. Soc.* **2011**, *133*, 9674; b) X. Huang, H. Zhang, C. Guo, Z. Zhou, N. Zheng, *Angew. Chem.* **2009**, *121*, 4902; *Angew. Chem. Int. Ed.* **2009**, *48*, 4808; c) Y. Yamauchi, T. Yokoshima, T. Momma, T. Osaka, K. Kuroda, *J. Mater. Chem.* **2004**, *14*, 2935; d) N. Zech, E. J. Podlaha, D. Landolt, *J. Electrochem. Soc.* **1999**, *146*, 2886; e) N. Zech, E. J. Podlaha, D. Landolt, *J. Electrochem. Soc.* **1999**, *146*, 2892.
[13] P. E. Levitz, *Colloids Surf. A* **2002**, *205*, 31.
[14] a) Ö. Çelik, Ö. Dag, *Angew. Chem.* **2001**, *113*, 3915; *Angew. Chem. Int. Ed.* **2001**, *40*, 3799; b) C. Li, T. Sato, Y. Yamauchi, *Angew. Chem.* **2013**, *125*, 8208; *Angew. Chem. Int. Ed.* **2013**, *52*, 8050; c) H. Wang, S. Ishihara, K. Ariga, Y. Yamauchi, *J. Am. Chem. Soc.* **2012**, *134*, 10819.
[15] a) L. Wang, Y. Yamauchi, *J. Am. Chem. Soc.* **2009**, *131*, 9152; b) H. Ataee-Esfahani, L. Wang, Y. Yamauchi, *Chem. Commun.* **2010**, *46*, 3684; c) H. Ataee-Esfahani, Y. Nemoto, L. Wang, Y. Yamauchi, *Chem. Commun.* **2011**, *47*, 3885.
[16] L. Wang, Y. Yamauchi, *Chem. Mater.* **2009**, *21*, 3562.
[17] H. Ataee-Esfahani, Y. Nemoto, M. Imura, Y. Yamauchi, *Chem. Asian J.* **2012**, *7*, 876.
[18] H. Ataee-Esfahani, L. Wang, Y. Nemoto, Y. Yamauchi, *Chem. Mater.* **2010**, *22*, 6310.
[19] a) Y. Zhang, M. Janyasupab, C. W. Liu, X. Li, J. Xu, C. C. Liu, *Adv. Funct. Mater.* **2012**, *22*, 3570; b) C. Xu, L. Wang, R. Wang, K. Wang, Y. Zhang, F. Tian, Y. Ding, *Adv. Mater.* **2009**, *21*, 2165.
[20] Y. Liu, M. Chi, V. Mazumder, K. L. More, S. Soled, J. D. Henao, S. Sun, *Chem. Mater.* **2011**, *23*, 4199.
[21] L. Liu, E. Pippel, R. Scholz, U. Gosele, *Nano Lett.* **2009**, *9*, 4352.
[22] a) N. Tian, Z. Y. Zhou, S. G. Sun, Y. Ding, Z. L. Wang, *Science* **2007**, *316*, 732; b) Z. Y. Zhou, Z. Z. Huang, D. J. Chen, Q. Wang, N. Tian, S. G. Sun, *Angew. Chem.* **2010**, *122*, 421; *Angew. Chem. Int. Ed.* **2010**, *49*, 411; c) S. W. Lee, S. Chen, W. Sheng, N. Yabuuchi, Y. T. Kim, T. Mitani, E. Vescovo, Y. Shao-Horn, *J. Am. Chem. Soc.* **2009**, *131*, 15669.